# Long-term Evolution of Large-scale Magnetic Fields in Rotating Stratified Convection

Youhei MASADA<sup>1</sup> and Takayoshi SANO<sup>2</sup> <sup>1</sup>Department of Computational Science, Kobe University; Kobe 857–8501; ymasada@harbor.kobe-u.ac.jp <sup>2</sup>Institute of Laser Engineering, Osaka University; Suita, Osaka 565–0871;sano@ile.osaka-u.ac.jp

(Received 17 February, 2014; accepted 25 March, 2014)

## Abstract

Convective dynamo simulations are performed in local Cartesian geometry. We report the first successful simulation of a large-scale oscillatory dynamo in rigidly rotating convection without stably stratified layers. A key requirement for exciting the large-scale dynamo is a sufficiently long integration time comparable to the ohmic diffusion time. By comparing two models with and without stably stratified layers, their effect on the large-scale dynamo is also studied. The spatiotemporal evolution of the large-scale magnetic field is similar in both models. However, it is intriguing that the magnetic cycle is much shorter in the model without the stable layer than with the stable layer. This suggests that the stable layer impedes the cyclic variations of the large-scale magnetic field.

Key words: Convection - turbulence - Sun: magnetic fields - stars: magnetic fields

## 1. Introduction

A grand challenge in astrophysics is to understand a selforganizing property of magnetic fields in highly turbulent flows. The solar magnetism is the front line of this area. The solar magnetic field shows a remarkable spatiotemporal coherence even though it is generated by turbulent convection operating within its interior. Our understanding on the solar magnetism has been accelerated over the past decade in response to the broadening, deepening and refining of numerical dynamo models (Charbonneau 2010; Brandenburg et al. 2012; Miesch 2012). However, it is still unclear what dynamo mode is excited in the solar interior and how it regulates the magnetic cycle.

Various geometries have been applied to the numerical dynamo modeling; global spherical shell geometry (e.g., Gilman & Miller 1981; Brun et al. 2004; Ghizaru et al. 2010; Masada et al. 2013), spherical-wedge geometry (e.g., Brandenburg et al. 2007; Käpylä et al. 2010), and local Cartesian geometry (e.g., Cattaneo & Vainshtein 1991; Brandenburg et al. 1996). Among them, the local Cartesian geometry is the most simplified one and is often used for distilling the physical essence of the convective dynamo process by more accurately resolving convective eddies.

A long-standing goal in the numerical dynamo modeling in the local Cartesian geometry is to realize the successful simulation of self-organized and self-sustained large-scale magnetic fields, so-called "large-scale dynamos", by rotating convection alone without mean shear flow. The mean-field dynamo theory predicts that the rigidly rotating convection can generate net helicity and then excite the large-scale dynamo even without the mean shear effect via a stochastic process, which is known as the  $\alpha$ -effect (Moffatt 1978; Krause & Raedler 1980). However, no evidence of the large-scale dynamo was found in earlier studies of the rigidly rotating convection (e.g., Cattaneo & Hughes 2006; Tobias et al. 2008). Käpylä et al. (2009) brought a breakthrough in the dynamo modeling in the local system. They were the first to demonstrate that the rigidly rotating convection can excite the largescale dynamo in the local system that consists of the convection layer and the stably stratified layers. Subsequently, the oscillatory behavior of the large-scale magnetic field was reported in Käpylä et al. (2013). Since the large-scale dynamo can be excited only when the Coriolis number is large, they concluded that the absence of the large-scale dynamo in earlier studies is caused by the slow rotation speed.

However, even in the sufficiently-rapid rotating convection, Favier & Bushby (2013) could not find the evidence for the large-scale dynamo in the local system with the convection zone alone. They suggested that the essential part for the largescale dynamo might be the stably stratified layer assumed in the model of Käpylä et al. (2009) rather than the rapid rotation.

Therefore, at present, the key requirement for the large-scale dynamo is still controversial. The purpose of this work is to find the evidence of the large-scale magnetic field in the system only with the convection zone in order to demonstrate that the rigidly rotating convection is a sufficient condition for the large-scale dynamo. In addition, by comparing two convective dynamo models with and without stably stratified layers, we will discuss their effect on the large-scale dynamo.

## 2. Model Setup

We numerically solve two convective dynamo systems in local Cartesian domain: one-layer system (Model A) only with convection zone of thickness d ( $z_1 \le z < z_2$ ), and three-layers system (Model B) consisting of upper isothermal cooling layer of depth 0.15d ( $z_0 \le z \le z_1$ ), middle convection layer of depth d ( $z_1 \le z < z_2$ ) and bottom stably stratified layer of depth 0.85d( $z_2 \le z < z_3$ ), where the x- and y-axes are taken to be horizontal and z-axis is pointing downward. The aspect ratio between

## Large-scale Dynamo in Rotating Stratified Convection

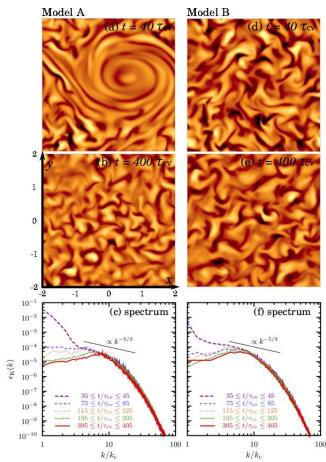


Fig. 1. Distribution of the radial velocity on the horizontal plane at the middle of the convection zone when (a)  $t = 40\tau_{\rm cv}$  and (b)  $t = 400\tau_{\rm cv}$  for the model A (panels (d) and (e) are those for the model B). Panels (c) and (f) are kinetic energy spectrum for the models A and B. Power-law slopes proportional to  $k^{-5/3}$  are shown for reference.

the thickness of the convection layer and the box width (W) sets to be W/d = 4 for both models. The setups in the models A and B are similar to those used in Favier & Bushby (2013) and Käpylä et al. (2009), respectively.

The basic equations are the compressible MHD equations in the rotating frame of reference with a constant angular velocity  $\Omega = -\Omega_0 e_z$ 

$$\frac{\partial \rho}{\partial t} = -\nabla \cdot \left(\rho \boldsymbol{u}\right),\tag{1}$$

$$\frac{D\boldsymbol{u}}{Dt} = -\frac{\nabla P}{\rho} + \frac{\boldsymbol{J} \times \boldsymbol{B}}{\rho} - 2\boldsymbol{\Omega} \times \boldsymbol{u} + \frac{\nabla \cdot \boldsymbol{\Pi}}{\rho} + \boldsymbol{g} , \qquad (2)$$

$$\frac{D\epsilon}{Dt} = -\frac{P\nabla \cdot \boldsymbol{u}}{\rho} + \mathcal{Q}_{\text{heat}} - \frac{\epsilon - \epsilon_0}{\tau(z)} , \qquad (3)$$

$$\frac{\partial \boldsymbol{B}}{\partial t} = \nabla \times \left( \boldsymbol{u} \times \boldsymbol{B} - \eta_0 \boldsymbol{J} \right), \tag{4}$$

where  $J = \nabla \times B/\mu_0$  is the current density,  $g = g_0 e_z$  is the gravity,  $\epsilon$  is the specific internal energy. The viscosity, magnetic diffusivity, and thermal conductivity are represented by  $\nu_0$ ,  $\eta_0$ , and  $\kappa_0$ , respectively. The last term in equation (3) works only in the model B and describes a cooling at the top of the domain with the cooling time  $\tau(z)$  which has a smooth profile

connecting to the convection layer, where  $\tau(z_1) = \infty$ .

The viscous stress  $\Pi$  is written by  $\Pi = 2\rho\nu_0 S$  with the strain rate tensor

$$S_{ij} = \frac{1}{2} \left( \frac{\partial u_i}{\partial x_j} + \frac{\partial u_j}{\partial x_i} - \frac{2}{3} \delta_{ij} \frac{\partial u_i}{\partial x_i} \right) \,. \tag{5}$$

The heating term  $Q_{heat}$  consists of the thermal conduction, viscous heating and Joule heating,

$$Q_{\text{heat}} = \frac{\nabla \cdot (\kappa_0 \nabla \epsilon)}{\rho} + 2\nu_0 S^2 + \frac{\mu_0 \eta_0 J^2}{\rho} \,. \tag{6}$$

We assume a perfect gas law  $P = (\gamma - 1)\rho\epsilon$  with  $\gamma = 5/3$ .

The initial hydrostatic balance is described by a piecewise polytropic distribution with the polytropic index m,

$$\frac{\mathrm{d}\epsilon}{\mathrm{d}z} = \frac{g_0}{(\gamma - 1)(m+1)} \,. \tag{7}$$

We choose m = 1 for the convection layer, and m = 3 for the stable layer. The thermal conductivity is determined by requiring a constant vertical heat flux throughout the domain.

Normalization quantities are defined by setting  $d = g_0 = \rho_0 = \mu_0 = 1$ , where  $\rho_0$  is the initial density at  $z = z_0$ . The velocity normalization corresponds to  $\sqrt{dg_0} = 1$ . The stratification level is controlled by the normalized pressure scale height at the surface defined by  $\xi = H_p/d = (\gamma - 1)\epsilon_0/(g_0d)$ , where  $\epsilon_0$  is the specific internal energy at  $z = z_0$ . In this work, we use  $\xi = 0.3$ , yielding a density contrast between top and bottom of the convection zone about 5.

We define the Prandtl, magnetic Prandtl, and Rayleigh numbers by

$$\Pr = \frac{\nu_0}{\chi_0} , \ \Pr = \frac{\nu_0}{\eta_0} , \ \operatorname{Ra} = \frac{g_0 d^4}{\chi_0 \nu_0} \left[ \frac{\nabla - \nabla_{\mathrm{ad}}}{H_p} \right] , \tag{8}$$

where  $\chi_0 \equiv \kappa_0/\gamma\rho$  is the thermal diffusivity,  $\nabla - \nabla_{ad}$  is the superadiabatic temperature gradient with  $\nabla_{ad} = 1 - 1/\gamma$ ,  $\nabla = (\partial \ln T/\partial \ln P)$ , and  $H_p$  is the pressure scale height. The variables  $(\rho, \nabla, \text{ and } H_p)$  in equation (8) are evaluated at the mid-convection zone of the depth  $z_m = (z_2 - z_1)/2$ .

In the following, the volume average in the convection zone and the horizontal average are denoted by single angular brackets with subscript "v" and subscript "h", respectively. The time-average of each spatial mean is denoted by additional angular brackets. The relative importance of rotation to the convection is measured by the Coriolis number  $\text{Co} = 2\Omega_0 d/u_{\text{cv}}$ , where  $u_{\text{cv}} \equiv \sqrt{\langle \langle u_z^2 \rangle \rangle_{\text{v}}}$  is the mean convective velocity. The convective turn-over time and the equipartition field strength are defined, respectively, by  $\tau_{\text{cv}} \equiv d/u_{\text{cv}}$  and  $B_{\text{eq}} \equiv \sqrt{\langle \langle \mu_0 \rho u^2 \rangle \rangle_{\text{v}}}$ .

In the horizontal directions, all the variables are assumed to be periodic. Stress-free boundary conditions are used in the vertical direction for the velocity. Perfect conductor and vertical field boundary conditions are used for the magnetic field at the bottom and top boundaries, respectively. A constant energy flux which drives the convection is imposed on the bottom boundary. The internal energy is fixed on the top boundary.

The equations (1)–(6) are solved by the second-order Godunov-type finite-difference scheme which employs an approximate MHD Riemann solver developed by Sano et al.

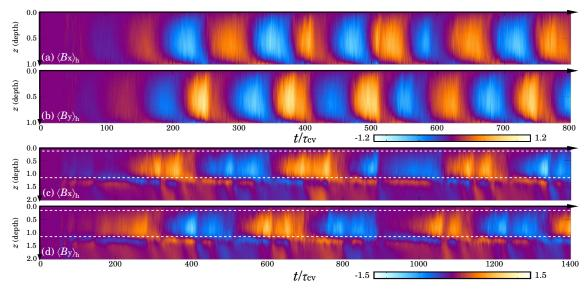


Fig. 2. Time-depth diagram of the horizontally-averaged horizontal magnetic field. Panels (a) and (b) [(c) and (d)] demonstrate  $\langle B_x \rangle_h$  and  $\langle B_y \rangle_h$  normalized by  $B_{eq}$  for the model A [model B]. The orange and blue tones denote the positive and negative strengths of the magnetic field.

(1998). The magnetic field evolution is calculated with CMoC-CT method (Clarke 1996). Non-dimensional parameters Pr =1.4, Pm = 4.0,  $Ra = 3.9 \times 10^6$ , constant angular velocity of  $\Omega_0 = 0.4$  and the same grid spacing are adopted for both models. The total grid size is 256 (in x) ×256 (in y) × 64 (in z) for the model A, and 256 (in x) ×256 (in y) × 128 (in z) for the model B. A small random perturbation is added to the velocity and magnetic fields when the calculation starts.

#### 3. Simulation Results

### 3.1. Properties of Convective Dynamo

After the convective motion sets in, the system reaches a saturated state at  $t \simeq 250\tau_{\rm cv}$  for both models. The mean convective velocity is evaluated there as  $u_{\rm cv} = 0.017$  (0.019), providing  $B_{\rm eq} = 0.045$  (0.045), Co = 47 (42) and  $\tau_{\rm cv} = 58.8$  (52.6) for the model A (model B). Since a sufficient scale separation between the convective eddies and the box scale is known as a necessary ingredient for the large-scale dynamo (e.g., Brandenburg & Subramanian 2005; Käpylä et al. 2009), we have chosen the relatively rapid rotation (Co $\gtrsim$  40), yielding small convective cells relative to the box scale.

Shown in Figure 1 is the distribution of the radial velocity in the horizontal plane at  $z = z_m$  when (a)  $t = 40\tau_{cv}$  and (b)  $t = 400\tau_{cv}$  for the model A [panels (d) and (e) are those for the model B]. The darker and lighter tones depict downflow and upflow velocities. In Figure 1(c) and (f), the temporal evolutions of two-dimensional kinetic energy spectra for the models A and B are shown. Note that a two-dimensional Fourier spectrum of the kinetic energy at the each depth is projected onto a one-dimensional wavenumber  $k^2 = k_x^2 + k_y^2$  and then is averaged over the convection zone and the time span shown in the figure legend. The different lines correspond to different time spans. The horizontal axis is normalized by  $k_c = 2\pi/W$ .

In the kinematic phase of the model A (left top), we can find the appearance of large-scale vortices, which have been discovered in earlier studies of rotating convections (e.g., Chan 2007). In this phase, the spectrum has a peak at  $k/k_c = 1$  (purple longdashed line). As found by Käpylä et al. (2013), the large-scale vortices decay as the magnetic fields grow, and finally disappears at the saturated phase. In the saturated phase, the convective motion is characterized by the broader and slower upflow surrounded by narrower and faster downflow lanes. The spectrum has a peak at around  $k/k_c \simeq 6$  for both models. Since there is no physical mechanism for the symmetry breaking in the horizontal directions, mean horizontal shear flow is absent in our simulations. In contrast, a mean kinetic helicity naturally arises from the up-down asymmetry in the convective motion (e.g., Spruit et al. 1990). This could play a prominent role in sustaining large-scale dynamo in our systems.

Figure 2 depicts the time-depth diagram of horizontallyaveraged horizontal magnetic fields. Shown in panels (a) and (b) [(c) and (d)] are  $\langle B_x \rangle_{\rm h}(t,z)$  and  $\langle B_y \rangle_{\rm h}(t,z)$  normalized by  $B_{\rm eq}$  for the model A [model B]. The orange and blue tones denote the positive and negative strengths of the magnetic field. The region between white dashed lines in panels (c) and (d) corresponds to the convection layer. In the saturated phase of  $t \gtrsim 250\tau_{\rm cv}$ , the large-scale magnetic field is spontaneously organized in the bulk of the convection zone for both models. The strength of the large-scale field maximally exceeds  $B_{\rm eq}$  at the mid convection zone, and averagely is about 20% of the total field strength.

The large-scale magnetic field shows a well-regulated oscillatory behavior. The strong magnetic field appears at the middle of the convection zone and propagates from there to top and base of the convection zone for both models. It is intriguing that the oscillation period of the large-scale magnetic field is shorter in the model A than in the model B. The polarity is reversed with the period of about  $70\tau_{cv}$  for the model A and  $200\tau_{cv}$  for the model B. It is noteworthy that there is a phase difference of about  $\pi/2$  between  $\langle B_x \rangle_h$  and  $\langle B_y \rangle_h$ . The observed oscillatory behavior in the model B is similar to that seen in Käpylä et al. (2013), but its cycle period is about twice as long as that in their model.

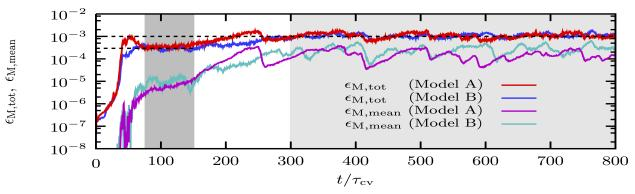


Fig. 3. Time-evolutions of the volume-averaged energy of the total magnetic field  $\epsilon_{M,tot} \equiv \langle B^2 \rangle_v / 2\mu_0$  (red line) and that of the mean-magnetic component defined by  $\epsilon_{M,mean} \equiv \langle B \rangle_v^2 / 2\mu_0$  (purple line) for the model A. The blue and cyan lines are those for the model B.

## 3.2. Two-Step Saturation Process of the Magnetic Field

In earlier studies of rigidly rotating convections, the largescale dynamo was not found in the system only with the convection zone (Cattaneo & Hughes 2006; Favier & Bushby 2013). Favier & Bushby (2013) suggested that the stably stratified layer, which was considered in Käpylä et al. (2009), might play a key role in organizing the large-scale magnetic field. However, in this work, the large-sale dynamo was excited regardless the presence of the stable layer. Then, a question naturally arises from our result "what is the crucial factor which makes a difference between our work and earlier studies ?".

To answer this question, we examine, in detail, the temporal evolution of the magnetic energy in Figure 3. The red line shows the volume-averaged energy of the total magnetic field  $\epsilon_{M,tot} \equiv \langle B^2 \rangle_v / 2\mu_0$  and the purple line is that of the meanmagnetic component defined by  $\epsilon_{M,mean} \equiv \langle B \rangle_v^2 / 2\mu_0$  for the model A. The blue and cyan lines are those for the model B.

Two saturation phases appear during the evolution of the magnetic energy. The first saturation phase is shaded by dark gray and the second one is by light gray. This would be strongly related to the evolution of the mean magnetic component. In the first saturation phase, the magnetic energy of the mean component is  $\mathcal{O}(100)$  times smaller than that of the turbulent component. The small-scale turbulent dynamo is thus supposed to be dominated in this phase. The large-scale component evolves slowly after the first saturation phase over the period of the time  $\sim 100\tau_{\rm cv}$ , and finally acquires a comparable strength to the turbulent field at around  $t = 250\tau_{\rm cv}$ .

This can be confirmed from the evolution of the spatial structure of the magnetic field. Figure 4 shows the distribution of the magnetic energy in the horizontal plane at the middle of the convection zone when (a)  $t = 100\tau_{cv}$  (first saturation phase) and (b)  $t = 330\tau_{cv}$  (second saturation phase) for the model A. The filamentary small-scale magnetic field prevails in the first saturation phase. It inversely cascades to the larger scale as time passes, and builds up the large-scale magnetic structure in the second saturation phase. The magnetic structure of the model B evolves in the same manner as that of the model A.

The evolution of the large-scale magnetic field seems to be characterized by magnetic diffusion time, which is evaluated as  $\tau_{\rm diff} \equiv d^2/\eta_0 \simeq 250\tau_{\rm cv}$  in our models. This indicates that the simulation should be evolved for a sufficiently long time comparable to the magnetic diffusion time to build up a significant large-scale magnetic field.

The resistively-dominated slow saturation of the large-scale magnetic field has been seen in the simulation of forced MHD turbulence with closed boundaries due to the magnetic helicity conservation (Brandenburg 2001). Although we have used vertical field (open) boundary condition that allows magnetic helicity fluxes out of the domain, it does not necessarily ensure that such fluxes are large enough to facilitate the evolution of the large-scale magnetic field. Even in the large-scale dynamos with open boundaries, the slow saturation has been observed (c.f., Brandenburg & Subramanian 2005; Käpylä et al. 2008).

In Favier & Bushby (2013), the integration time of their simulations is substantially shorter than the magnetic diffusion time. It would be possible that the absence of large-scale dynamos in their study is a simple consequence of their relatively short integration time. To specify all the requirements for building up large-scale magnetic fields in rigidly rotating turbulent convections, we should examine long-term evolutions of dynamos in wider parameter range. It is however not within the scope of this work and will be the subject of our future paper.

#### 4. Discussion & Summary

We performed rigidly rotating convective dynamo simulations in the local Cartesian geometry. By comparing two models with and without stably stratified layers, their effect on a large-scale dynamo was studied. We for the first time successfully simulated an oscillatory large-scale dynamo in the local system without the stable layer, whereas it was not found in the similar earlier studies (Cattaneo & Hughes 2006; Favier & Bushby 2013). The absence of large-scale dynamos in earlier studies might be a simple consequence of their relatively short integration time. For the excitation of the large-scale dynamo, we should evolve the simulation for a sufficiently long time because the large-scale magnetic component is gradually built up in an order of the ohmic diffusion time.

The spatiotemporal evolution of the magnetic field was similar in two models. The large-scale magnetic component was the strongest at around the middle of the convection layer and propagated from there to the upper and lower convection zones. According to the mean-field dynamo theory, the  $\alpha$ -effect would be solely responsible for the large-scale dynamo in our models

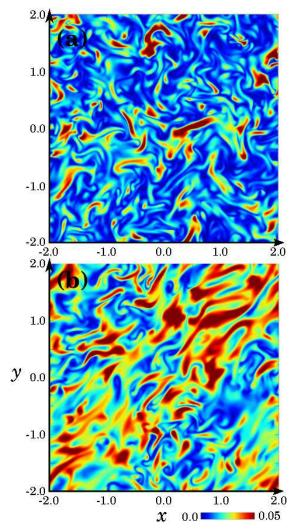


Fig. 4. Distribution of the magnetic energy on the horizontal plane at the middle of the convection zone when (a)  $t = 100\tau_{cv}$  (first saturation phase) and (b)  $t = 330\tau_{cv}$  (second saturation phase) for the model A.

because the  $\Omega$ -effect is absent in the rigidly rotating system (c.f., Käpylä et al. 2013). However, the nonlinear properties of the  $\alpha$ -effect dynamo in the natural rotating convection are still veiled in mystery. We will examine quantitatively whether the  $\alpha$ -effect dynamo can reproduce the spatiotemporal evolution of large-scale magnetic fields observed at the nonlinear saturated phase in our simulations in a subsequent paper.

An intriguing finding was the difference in the oscillation period of the large-scale magnetic field between two models. The magnetic cycle was about three-times longer in the model with the stable layer than without the stable layer, although the properties of the convective motion was similar in two models. This suggests that the stably stratified layer rather impedes the cyclic variation of large-scale magnetic fields. One possible cause making a difference in the cycle period is the ejection process of the magnetic helicity, which is known to affect nonlinear properties of dynamos (c.f., Blackman & Field 2000).

In the model without stable layers, the magnetic helicity can be ejected from the system via advective transport processes because the top open boundary is placed just above the convection zone. In contrast, in the model with the top stable layer, the magnetic field must be transported throughout the stable layer for the loss of the magnetic helicity. The relatively slow ohmic diffusion dominates the transport process there. We thus speculate that the smaller magnetic helicity flux dominated by the slower ohmic diffusion process is responsible for the longer cycle period in the model with stable layers.

The dynamo number and thus frequency of excited dynamo mode might be different between two models. This is because the mode with longer wavelength can be allowed in the system with conducting stable layers above and below the convection zone. This might be an another possibility to explain the cycle period difference (c.f., Rädler & Bräuer 1987; Rüdiger et al. 2003). In any case, further simulations with varying the thickness of the stable layers and the resistivity are necessary to elucidate the cause and will be a target of our future work.

We acknowledge the anonymous referee for constructive comments. Computations were carried on XC30 at NAOJ, and K-Computer at RIKEN. This work was supported by JSPS KAKENHI Grant number 24740125 and the joint research project of the Institute of Laser Engineering, Osaka University.

## References

- Blackman, E.G., & Field, G.B. 2000, ApJ, 534, 984
- Brandenburg, A., Jennings, R.L., Nordlund, Å., et al. 1996, J. Fluid. Mech., 306, 325
- Brandenburg, A. 2001, ApJ, 550, 824
- Brandenburg, A., & Subramanian, K. 2005, Phys. Rep., 417, 1
- Brandenburg, A., Käpylä, P.J., Mitra, D., Moss, D., & Tavakol, R. 2007, Astron. Nachr., 328, 1118
- Brandenburg, A., Sokoloff, D., & Subramanian, K. 2012, Space Sci. Rev., 169, 123
- Brun, A.S., Miesch, M.S., & Toomre, J. 2004, ApJ, 614, 1073
- Cattaneo, F., & Vainshtein, S. I. 1991, ApJL, 376, L21
- Cattaneo, F., & Hughes, D.W. 2006, J. Fluid. Mech., 553, 401
- Chan, K.L. 2007, Astron. Nachr., 328, 1059
- Charbonneau, P. 2010, Living Reviews in Solar Physics, 7, 3
- Clarke, D.A. 1996, ApJ, 457, 291
- Favier, B., & Bushby, P. 2013, J. Fluid. Mech., 723, 529
- Gilman, P.A., & Miller, J. 1981, ApJS, 46, 211
- Ghizaru, M., Charbonneau, P., & Smolarkiewicz, P.K. 2010, ApJL, 715, L133
- Käpylä, P.J., Korpi, M.J., & Brandenburg, A. 2008, A&A, 491, 353
- Käpylä, P.J., Korpi, M.J., & Brandenburg, A. 2009, ApJ, 697, 1153
- Käpylä, P.J., Korpi, M.J., Brandenburg, A., Mitra, D., & Tavakol, R. 2010, Astron. Nachr., 331, 73
- Käpylä, P.J., Mantere, M.J., & Brandenburg, A. 2013, Geophysical and Astrophysical Fluid Dynamics, 107, 244
- Krause, F., & Raedler, K.-H. 1980, Mean-field Magnetohydrodynamics and Dynamo Theory (Oxford: Pergamon).
- Masada, Y., Yamada, K., & Kageyama, A. 2013, ApJ, 778, 11
- Miesch, M.S. 2012, Royal Society of London Philosophical Transactions Series A, 370, 3049
- Moffatt, H.K. 1978, Magnetic field generation in electrically conducting fluids, Cambridge University Press, 1978. 353 p.
- Rädler, K.-H., & Bräuer, H.-J. 1987, Astron. Nachr., 308, 101
- Rüdiger, G., Elstner, D., & Ossendrijver, M. 2003, A&A, 406, 15
- Sano, T., Inutsuka, S., & Miyama, S.M. 1998, ApJL, 506, L57
- Spruit, H.C., Nordlund, A., & Title, A.M. 1990, ARA&A, 28, 263
- Tobias, S.M., Cattaneo, F., & Brummell, N.H. 2008, ApJ, 685, 596